TOWARDS A FRACTIONED TREATMENT IN CONFORMAL RADIOTHERAPY USING 3D-MULTIMODAL DATA REGISTRATION

R. Posada [1], Ch. Daul[1], D. Wolf [1], P. Aletti [2], R. Miranda [1]

[1]Centre de Recherche en Automatique de Nancy (CRAN, CNRS UMR 7039),
2 avenue de la Forêt de Haye, 54516 Vandœuvre-Les-Nancy, France.
[2]Centre Alexis Vautrin, Avenue de Bourgogne, 54511 Vandœuvre-Les-Nancy, France.

ABSTRACT

The combination of conformal radiotherapy and fractioned radiotherapy is a very useful tool against cancer. Meanwhile, this combination is only interesting if the patient positioning method is accurate and non invasive. This paper presents an algorithm fulfilling the latter conditions. The method was developed for tumors located in the head and does not need any patient dedicated device. Homologous structures, acquired with a computer tomograph and with a sensor fixed in the treatment room, are used to register two 3D-surfaces. The registration scheme is notably based on the directed Hausdorff distance. The registration, together with a calibration of the 3D-sensor in the therapy room, leads to a mean positioning error of 0.77 mm. Tests performed with a phantom deliver also a maximal error of 1.6 mm.

1. INTRODUCTION

The aim of any radiotherapy technique is to improve the carcinogenic cell destruction while reducing at best the undesirable effects onto the neighboring healthy tissue. One way to limit the sequels due to tissue irradiation is to spread the treatment over several sessions (fractioned radiotherapy; *FRT*). This method takes advantage of the fact that the regeneration of carcinogenic cells is slower and less efficient than the one of healthy cells. In the case of *FRT*, radiologists recommend short and daily sessions spread over several weeks so that only the healthy tissue regenerates. Unfortunately, the high precision of positioning needed in such radiotherapy techniques makes fractioned treatments complicated and expensive (especially for a large session number). To overcome these problems irradiation doses are voluntarily reduced and irradiated zones are increased so that the accuracy of patient positioning becomes less critical. The principle of another common protocol of treatment realized in one session is to increase the irradiation dose and to reduce the target volume. This method, called conformal radiotherapy (*CRT*), needs an accurate model of the incident radiation and a precise positioning of the patient in the radiotherapy room. The patient positioning method associated to *CRT* is frequently based on invasive methods and requires either stereotactic frames or implanted markers [1], [2]. Many attempts have been made in the field of *CRT* to find less invasive positioning methods. Most of them either need radical changes in the organization of the treatment room [3] or use less contrasted images like portal images so that many interventions of radiologists are required [4], [5].

Recently, a new interesting patient positioning method, based on the use of infrared LEDs and spherical markers fixed onto a dental support blocked between the maxillary dentition of the patient, was proposed [6]. The mean tumor positioning error of this method is about 1.1 mm. This approach can be used in *FRT*. Meanwhile, patient dedicated devices are needed (molded bite plate system), and the treatment becomes more complex for radiologists. This paper presents a non invasive method of patient positioning that can be used for both *CRT* and *FRT* and that does not need any patient dedicated device. The method requires only patient internal landmarks and was applied to lesions located in the head. Moreover, the proposed algorithm was conceived with the intent to modify as less as possible the different steps of traditional treatment methods for taking into account radiologist habits.

2. METHODOLOGY

At least one data acquisition, using e.g. computer tomography (CT), is always realized for both *CRT* and *FRT*. The acquired data, used usually to determine the 3D-dosimetry, are obviously given in the CT-coordinate system ($O_{CT}, \vec{x}_{CT}, \vec{y}_{CT}, \vec{z}_{CT}$). The patient must be positioned accurately in the coordinate system ($O_m, \vec{x}_m, \vec{y}_m, \vec{z}_m$) of the irradiation machine located in the treatment room, O_m being the machine isocentre where all ionizing beams converge. The mathematical problem related to the patient positioning task lies in the exact superimposition of the two coordinate systems. For the more or less invasive methods mentioned in the previous section, this

0-7803-8554-3/04/$20.00 ©2004 IEEE.

superposition is realized using a third coordinate system related either to a stereotactic frame or to patient internal or external landmarks. For the proposed non invasive positioning algorithm, the third coordinate system, called ($O_{3DS},\vec{x}_{3DS},\vec{y}_{3DS},\vec{z}_{3DS}$), corresponds to the one of a sensor based on the structured light principle. This sensor, fixed in the treatment room, acquires 3D-points spread out over the patient's face. The positioning problem is solved by finding the geometrical transformation superimposing exactly the patient's face data (surface defined by a 3D-point cloud of the visible light modality) with the patient's head data (3D-point cloud of the CT-modality and distributed over the whole patient's head). The transformation between the CT- and the machine coordinate systems, based on the previous mentioned patient information, is determined with a two-step algorithm.

Step 1: link between the sensor and the irradiation machine coordinate systems ($O_{3DS},\vec{x}_{3DS},\vec{y}_{3DS},\vec{z}_{3DS}$) and ($O_m,\vec{x}_m,\vec{y}_m,\vec{z}_m$). This transformation consists of 3D-rotations and translations. The parameters of the corresponding matrix are computed with data acquired by the 3D-sensor and related to a calibration piece specially designed for classical therapy machines. This calibration piece is built in such a way that the positions of four points are exactly known in ($O_m,\vec{x}_m,\vec{y}_m,\vec{z}_m$). The positions of these points are also accurately measured in ($O_{3DS},\vec{x}_{3DS},\vec{y}_{3DS},\vec{z}_{3DS}$). The transformation matrix can be analytically determined knowing the correspondence between three points in the two coordinate systems. The fourth point represents redundant information used to check the calibration parameters. The principle of the calibration is sketched in Fig. 1.

Step 2: link between the CT- and sensor coordinate systems ($O_{CT},\vec{x}_{CT},\vec{y}_{CT},\vec{z}_{CT}$) and ($O_{3DS},\vec{x}_{3DS},\vec{y}_{3DS},\vec{z}_{3DS}$). The two data sets delivered by the CT-scan and the 3D-sensor represent homologous structures used in a multimodal registration scheme mathematically formulated in (1). D_m and D_t are respectively the 3D-point sets of the visible light modality and of the CT-modality. $\tilde{T}$ corresponds to the transformation T minimizing (or maximizing) the measure of similarity S. f_m and f_t are typically segmentation algorithms necessary when D_m and D_t are not directly usable for the registration.

$$\tilde{T} = \underset{T}{arg\,opt}\, S\left(f_m(D_m), T\left(f_t(D_t)\right)\right) \qquad (1)$$

In the practical case of patient positioning, equation (1) is applied as follows.

- D_t is the data set transformed by T. The latter data must match at best the model data set D_m.
- T is an isometry. This transformation type was chosen under the assumption that a patient can take a same neutral expression during the acquisition of D_m and D_t.

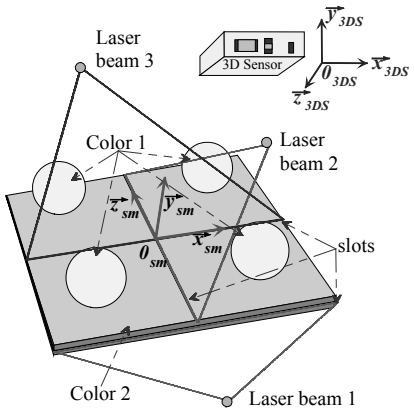

Fig. 1. Calibration step. Three laser beams sweep three orthogonal planes in the treatment room. The plane intersections result in three axes and one point O_m defining the orthogonal coordinate system ($O_m,\vec{x}_m,\vec{y}_m,\vec{z}_m$) of the radiotherapy machine. The calibration piece consists of four spheres fixed onto a plate in which orthogonal slots are machined. The piece is positioned so that the laser planes fall into the slots. In this situation, the position of the four spheres are exactly known in ($O_m,\vec{x}_m,\vec{y}_m,\vec{z}_m$). An acquisition of the calibration piece is then realized with the 3D-sensor. A segmentation algorithm based on the coordinates and the color information delivered for each point by the sensor permits to associate the 3D-points either to the plate or to one of the spheres. The coordinates of the sphere centres are finally computed in ($O_{3D},\vec{x}_{3D},\vec{y}_{3D},\vec{z}_{3D}$).

-The direct Hausdorff distance (*DHD*) was chosen to measure the similarity between D_m and D_t (see equation (2)). $h(D_m,D_t)$ is the greatest distance of all smallest distances from a 3D-point a of D_m to all points b of D_t. The *DHD* was chosen according criteria such as data type to register, type of T, robustness against perturbations, *etc*.

$$h(D_m,D_t) = \max_{a\in D_m}\min_{b\in D_t}\|a-b\| \qquad (2)$$

- To obtain $\tilde{T}$, a steepest gradient and a simplex algorithm were sequentially used. The first algorithm converges quickly to the global minimum of the parameter space. The small and uninteresting local minima are avoided by giving a big value to the step size parameter. The simplex algorithm delivers then an accurate solution for an initialization close to the solution.
- D_m and D_t were directly suitable for the proposed registration algorithm. Nevertheless, for reducing in a drastic way the computation time, the most important points for the registration (points with a high curvature) were extracted from D_m. This down sampling algorithm (f_m in equation (1)) uses the Fan-method [7].

The principle, the advantages and the limits of the registration algorithm are detailed in [8]. The authors quantified the accuracy of the registration by comparing the parameters of a known transformation *Ti* (this

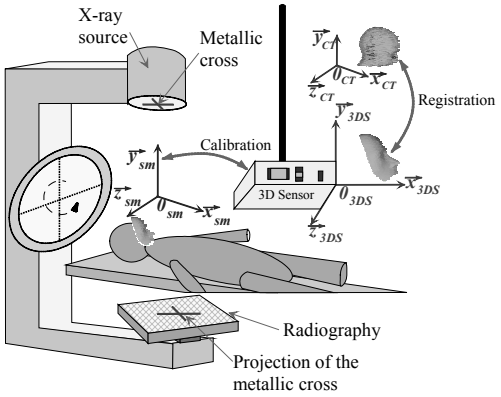

Fig. 2. Geometry of the simulation room. Two control radiographies are usually taken before a treatment (see Fig. 3). For these two acquisitions, the axis passing through the X-ray point source and the coordinates of the centre of the metallic cross is perpendicular to the radiography planes and to the axis pairs ($\vec{x}_{sm}, \vec{y}_{sm}$) of the first viewpoint and ($\vec{z}_{sm}, \vec{y}_{sm}$) of the second viewpoint. The projection of the axis pairs is visualized by the projection of the metallic cross into the radiographies. The distances "X-ray source / metallic cross centre (MCC)" and "MCC / radiographic plane" are also known.

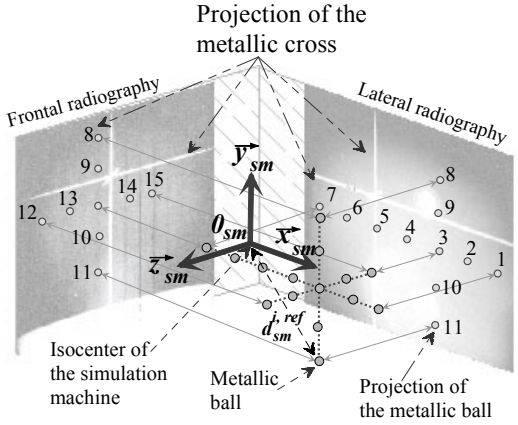

Fig. 3. Control radiographies. The numbers of the metallic balls correspond to the *i*-values table 1.

transformation was applied to a data set Dm acquired with the 3D-sensor) with the parameters of $\tilde{T}$ obtained with the registration algorithm. The greatest errors were about 1° and several hundredth of millimeters for respectively the three rotations and translations of $\tilde{T}$. The latter errors correspond to a mean positioning error of registered 3D-points (mean euclidean distance between the model points and the points transformed with $\tilde{T}$) of 0.03 mm. It must be noticed that these results were given for monomodal data to evaluate the errors inherent to the registration. The registration of the two multimodal data sets led to greater errors. The given results did also not include the errors due to the calibration. In the next section, an experiment for testing the accuracy of the whole positioning procedure (including the calibration and the multimodal data registration) is presented.

3. EXPERIMENT AND RESULTS

Tests were realized in a simulation room for evaluating the accuracy of the proposed algorithm. Such a room is useful for simulating a treatment (patient position, dose distribution, *etc*.) and is geometrically identical to the treatment room. The simulation and treatment rooms are fitted out by similar devices. In particular, the isocentre of the simulation machine is also visualized and defined by three laser beams (see Fig. 1). The major difference between the two rooms lies in the employed energy of the irradiation source. The linear accelerator of the treatment room is characterized by a high energy whereas the source of the simulation machine is suited to the realization of radiographic films (control radiographies). Such radiographies are generally taken for two well-defined viewpoints (see Figs. 2 and 3). Thus, the plane of the first radiography is parallel to the plane defined by the axis pair ($\vec{x}_{sm}, \vec{y}_{sm}$) while the second radiography is parallel to the plane ($\vec{z}_{sm}, \vec{y}_{sm}$), ($O_{sm}, \vec{x}_{sm}, \vec{y}_{sm}, \vec{z}_{sm}$) being the coordinate system of the simulation machine. Moreover, a metallic cross is fixed in front of the X-ray source so that the projections of the metallic cross onto the radiographies correspond exactly to the projections of the previous axis pairs onto the film planes.

The tests in the simulation room were performed with a plaster head. Fifteen metallic balls (simulating tumors) were included in the phantom. These radio-opaque balls, with a diameter of 2 mm, were regularly spaced and placed on three orthogonal axes (see Fig. 3). The following four-step experiment was realized with the plaster head.

1. Computation of the ball positions in the CT coordinate system. A scan was performed with the plaster head placed in the CT. The balls were spread out on several voxels of the CT. The barycentre positions ($x^i_{CT}, y^i_{CT}, z^i_{CT}$) are computed for each ball p_i ($i \in [1, 15]$).

***2. 3D*-sensor calibration**. The transformation matrix between the 3D-sensor coordinate system and the coordinate system of the simulation machine was determined with the method sketched in Fig. 1. Thus, the origin position of the 3D-sensor coordinate system is notably known in ($O_{sm}, \vec{x}_{sm}, \vec{y}_{sm}, \vec{z}_{sm}$). This origin has the coordinates ($x^{O3D}_{sm}, y^{O3D}_{sm}, z^{O3D}_{sm}$).

3. Data registration. An acquisition of the face of the plaster head placed onto the machine table was performed with the 3D-sensor in the simulation room. The CT-head data of step 1 were registered with the face data for finding the transformation $\tilde{T}$. The latter and the

barycentres ($x^i_{CT}, y^i_{CT}, z^i_{CT}$) permitted to compute the positions ($x^i_{3D}, y^i_{3D}, z^i_{3D}$) of each ball p_i in ($O_{3D}, \vec{x}_{3D}, \vec{y}_{3D}, \vec{z}_{3D}$). The distance $d^{i,com}_{sm}$ of a ball p_i to the origin of ($O_{sm}, \vec{x}_{sm}, \vec{y}_{sm}, \vec{z}_{sm}$) was then determined as follows :

$$d^{i,com}_{sm} = \sqrt{\left(x^i_{3D} - x^{O_{3D}}_{sm}\right)^2 + \left(y^i_{3D} - y^{O_{3D}}_{sm}\right)^2 + \left(z^i_{3D} - z^{O_{3D}}_{sm}\right)^2} \quad (3)$$

4. Realization of the control radiographies. Two control radiographies were acquired in the simulation room for the phantom (the position of the latter is the same than for step 3). The coordinates ($x^{i,proj}_{sm}, y^{i,proj}_{sm}, z^{i,proj}_{sm}$) of the projections of the balls p_i were then measured with a millimeter ruler on the radiographic films. Knowing the geometry of the simulation room, it was possible to reconstruct the reference positions ($x^{i,ref}_{sm}, y^{i,ref}_{sm}, z^{i,ref}_{sm}$) of the balls in ($O_{sm}, \vec{x}_{sm}, \vec{y}_{sm}, \vec{z}_{sm}$) using a projective model. This procedure is obviously affected by small measuring errors. However, it represents the reference method for patient position verification before a treatment. Moreover it was the only available solution for computing the reference distances $d^{i,ref}_{sm}$ which can be compared to the computed distances.

Table 1 provides $d^{i,ref}_{sm}$ and $d^{i,com}_{sm}$ values and their absolute differences ε_i for the fifteen balls. The mean positioning error and the standard deviation equal 0.77 mm and 0.38 mm respectively. The value of the greatest error (ball p_7) is 1.6 mm. One can notice here that the $d^{i,ref}_{sm}$ values are affected by different errors since the two radiographies are in fact not exactly orthogonal (1° error), the X-ray source is not in an exactly known position, *etc*. The real errors should probably be smaller than those given in table 1. Finally, no dependency between the error values and the ball positions in the head was noticed.

i	$d^{i,com}_{sm}$	$d^{i,ref}_{sm}$	$\varepsilon_i = \left\lvert d^{i,com}_{sm} - d^{i,ref}_{sm} \right\rvert$
1	105.52	104,39	1,13
2	80.79	80,03	0,76
3	56.89	56,33	0,56
4	35.38	34,49	0,89
5	18.06	18,22	0,16
6	28.09	27,41	0,68
7	50.40	48,80	1,60
8	64.84	63,65	1,19
9	54.96	55,07	0,11
10	68.07	67,45	0,62
11	84.51	83,96	0,55
12	69.20	69,75	0,55
13	60.68	60,23	0,45
14	58.50	59,24	0,74
15	65.64	65,02	0,62

Table 1. Ball positioning results. All values are given in millimeters.

4. CONCLUSION

The proposed positioning method seems to be promising since the reached accuracy is better than the one of the least invasive and most accurate algorithm of the literature [6]. Moreover, the proposed algorithm permits to combine *FRT* and *CRT* since it is non invasive and accurate and does not need any patient dedicated devices. However, a clinical validation must be realized by comparing for enough patients the obtained results with the ones of a frame based method for example.

5. REFERENCES

[1] K. P. Gall, L. J. Verhey, and M. Wagner, "Computer-assisted positioning of radiotherapy patients using implanted radiopaque ducials", *Med. Phys*., vol. 20, No 4, pp. 1153-1159, 1993.

[2] E. Vigneault, J. Pouliot, J. Laverdiere, J. Roy, and M. Dorion, "Electronic portal imaging device detection of radioopaque markers for the evaluation of prostate position during megavoltage irradiation: a clinical study", *Int. J. Radiation Oncology Biol. Phys*, vol. 37, No 1, pp. 205-212., 1997.

[3] M. Uematsu, A. Shioda, A. Suda, T. Fukui, Y. Ozeki, Y. Hama, J. R. Wong and S. Kusano, "Computed tomography-guided frameless stereotactic radiotherapy for stage I non-small-cell lung cancer : a 5-year experience", *Int. J. Radiation Oncology Biol. Phys*., vol. 51, No. 3, pp. 666-670, 2001.

[4] B.L. Phillips, M.R. Jiroutek, G. Tracton, M. Elfervig, K.E. Muller, and E.L. Chaney, "Thresholds for human detection of patient setup errors in digitally reconstructed portal images of prostate fields", *Int. J. Radiation Oncology Biol. Phys*, vol. 54, pp. 270-277, 2002.

[5] S. Clippe, D. Sarrut, C. Malet, S. Miguet, C. Ginestet, C. Carrie, "Patient setup error measurement using 3D intensity-based image registration techniques", *Int. J. Radiation Oncology Biol. Phys.*, vol. 56, No. 1, pp. 259-265, 2003.

[6] S. L. Meeks, F. J. Boba, T. H. Wagner, J. M. Buatti, W. A. Friedman, K. D. Foote, "Image localization for frameless stereotactic radiotherapy", *Int. J. Radiation Oncology Biol. Phys.*, Vol 46, No. 5, pp. 1291-1299, 2000.

[7] E. A. Pollard and R. C. Barr, "Adaptive sampling of intracellular and extracellular potentials with the Fan method", *Med. Biol. Eng. Comp*., vol. 25, pp. 261-268, 1987.

[8] R. Posada, Ch. Daul and D. Wolf, "New frameless patient positioning algorithm in conformal radiotherapy using 3D-data registration". *In Proceedings of the 25th Annual International Conference of the Biomedical Engineering Society IEEE/EMBS,* pp.152-156, Cancun, Mexico, 17-21 September 2003.

Acknowledgments. This work was partially sponsored by the ECOS-program, the CONACYT and the "Centre Alexis Vautrin" of Nancy.